Multiobjective Pareto Optimal Design of a Clutch System

O. Ozansoy[*‡], T. Tevruz[**], A. Mugan[**]

[*] : Istanbul Technical University, Faculty of Mechanical Engineering, Gumussuyu 34437, Istanbul, Turkey, Ford Otomotiv Sanayi A.Ş. Gebze Engineering, Tubitak Technopark, 41470 Gebze, Kocaeli

[**] : Istanbul Technical University, Faculty of Mechanical Engineering, Gumussuyu 34437

(oozansoy@ford.com, tevruz@itu.edu.tr, mugan@itu.edu.tr)

[‡] Corresponding Author; Onur Ozansoy, Ford Otomotiv Sanayi A.Ş. Gebze Engineering, Tubitak Technopark, 41470 Gebze, Kocaeli, oozansoy@ford.com

Abstract- Optimum design of a clutch and dual mass flywheel system is completed. Although the clutch systems are exposed to both rotational and axial vibrations, they are generally designed by considering rotational vibrations of engines and they do not have any component to damp axial vibrations due to the following two reasons: first, the package area of the clutch system is very limited and there is no available space to put additional springs and dampers to reduce these vibrations. Second, axial vibrations are normally insignificant to be considered in the analyses and such vibrations are supposed to be damped by the diaphragm spring and cushion springs. Nonetheless, axial vibrations may lead to some unexpected problems in the power train such as the rattle noise that is examined in this study by using global optimization techniques. The components in the clutch system are modeled analytically. Then, by considering the pedal characteristics and vibrations of pressure plate as objective functions, a multi-objective Pareto optimization problem is solved. It is shown that analytical models agree well with the experimental measurements and vibrations in the clutch system can be reduced significantly by choosing the design parameters with optimization tools.

Keywords Optimization; pareto optimality; dynamic systems; vibration; clutch.

1. Introduction

Since engineering structures are mostly subjected to dynamic loads, it is important to design these structures in consideration of their dynamic behavior whose optimization is difficult since the associated mathematical models are complicated and computational costs are expensive. In this study, dynamic behavior of a clutch and dual mass flywheel (DMF) system is optimized.

The clutch and dual mass flywheel system existing in manual transmissions of internal combustion engines are important components in a vehicle that affect the ride comfort of the vehicle and may cause noise, fatigue of components and longitudinal vibrations during the cruise of the vehicle. It is noteworthy that the loading on the clutch and dual mass flywheel system is transient and a dynamic model has to be employed in optimization studies. The clutch systems are essentially designed for damping out rotational vibrations of the engine; thus, it helps increase the ride comfort; nonetheless, they are exposed to axial vibrations as well. They generally do not have any component to annihilate axial vibrations due the following reasons: first of all, packaging area of the clutch system is limited between engine and transmission and there is no available space to add some springs and dampers to annihilate axial vibrations. Second of all, axial vibrations are normally insignificant to be considered in design phase which are supposed to be damped by the diaphragm spring and cushion springs. But, axial vibrations may lead to some unexpected results in the power train such as the rattle noise that is examined in this study by using global optimization techniques.

Many studies on the clutches of different types exist in literature. For instance, wet clutches and dual clutches, which are mostly used on automated manual transmissions,

engagement characteristics and their effects on engine characteristics, shift characteristics and their effects on shaft vibrations, modal frequencies of the clutch system and clutch control mechanisms are some of the investigation topics [1-7]. There are also studies in literature on modeling of one way clutches [8-9]. Manual transmission dry clutch systems and their rotational behavior are examined by some researchers [10-18, 41-42]. For example, Crowther and Zhang studied the torsional behavior of the clutch as an elastic system in the driveline [11]. Duan and Singh formulated the clutch engagement and disengagement as a nonlinear dry friction problem with harmonically varying normal load and investigated the stick-slip motions to understand the clutch response under various torque inputs [12-13]. Awrejcewicz and Grzelczyk studied the wear of clutch friction surfaces [18]. Being one of the most important component of a clutch system, the diaphragm spring (which determines clutch pedal load) is studied by some researchers and optimized for the best release load and durability [19-25]. Some researchers studied the Almen-Laszlo formula (which is used to calculate disc spring characteristics) [26] to improve its accuracy [27-30]. Information about main components of a clutch system can be found in [31-32].

One of the rare investigations on longitudinal vibrations in a clutch system is presented in [33] where Esfahani et al studied in-cycle vibrations on the clutch pedal which is excited by the crank shaft's axial vibration; at this point, the authors remark about the same challenge as we faced in this study which is the lack of an extensive axial clutch vibration studies in literature whilst the problem observed are connected with axial clutch vibrations. They focused on the clutch pedal vibrations around 257Hz, which is originated from the clutch axial vibrations, and their simulation showed the same vibration level around 230-240Hz which is a good correlation with actual condition, e.g., see [33]. But they did not investigate why their system showed the whoop frequency, or in cycle vibration, around 250Hz and did not present a discussion or proposal how this could be reduced. They only suggested using such kind of simulation toolboxes to foresee any possible problems before handling the physical parts.

Reitz et al. worked on a special test bench to investigate NVH problems in a clutch system [46]. They reported that the clutch system is excited by torsional and axial flywheel vibrations. Torsional flywheel vibrations are caused by the 2nd engine order and axial flywheel vibrations are caused by the crankshaft bending vibrations which are excited by the 4th cylinder firing. This means that axial vibrations are caused by the 0.5th engine order which is the same outcome of our investigations as explained in upcoming sections in detail. They also reported the test results of three different clutches but did not share the clutches' specifications due to confidentiality requirements. They presented their test bench that enables to determine the clutch systems NVH behavior during engagement and disengagement in detail and allow them to predict the behavior of the clutch system in a real vehicle.

Kelly and Rahnejat investigated the pedal vibrations and influence of individual components on the transmission of the subsequent vibration and noise [47]. They investigated the vibrations in a vehicle and multi-body model of clutch and observed that the pedal vibration and noise occurred due to the 0.5th engine order excitation from the 4th cylinder firing resulting in bending of the crankshaft. This is actually the same root cause of the clutch axial vibrations investigated in this study and although the source is the crankshaft bending vibrations, these vibrations are transmitted by the flywheel and clutch system. They also showed that cable properties and mass fixes can influence the vibrations.

Hasabe and Seiki studied the clutch pedal vibrations which are excited by the clutch axial vibrations [48]. They conducted an experimental study based on an on-vehicle observation of the vibrations and a test bench. They tried to develop a method for a test bench evaluation to predict the levels of vibration and noise in a vehicle having a 4 cylinder engine and observed that the pedal vibrations exist at 4400RPM engine speed when the clutch is half engaged and in the 1st, 3rd and 6th harmonic of the engine vibration. They observed the same behavior on the clutch side which proves that the vibrations are transmitted by the clutch system. They also stated that the clutch system has the major contribution on pedal vibrations. Their measurements showed that their sample clutch has the critical resonance frequency between 200-300Hz. Unlike other studies in literature, since their investigation covered the whole range of release bearing travel, they observed a relatively larger range for critical frequency and they proposed two different clutch behaviors at engaged and disengaged positions which lead to this larger range. They built a correlation between the vibration level and frequency range of two different natural frequencies of engaged and disengaged positions as well.

If the clutch model and its optimization are put aside, there are many studies related to gear rattle phenomenon in literature [14-15, 34-38]. Some of these studies focused on neutral gear rattle [34-35], some of them focused on backlash effects [15, 36-37]. Barthod et al. studied gear rattle phenomenon to understand the rattle threshold and rattle noise evolution in relation with excitations and mechanical gearbox parameters [38]. On the other hand, ergonomic issues of the clutch pedal characteristic for different driver profiles are studied in [39]. There are also some studies to identify the heat energy generation in friction clutch systems. To this end, Shabibi investigated the transient solution of heat conduction problem in solids with insulated boundaries [40].

Padmanabhan and Singh [14] employed a simplified rotational clutch model and showed that if clutch parameters are selected appropriately, it can help reduce the transmission rattle noise; although they employed a simplified clutch model, it is a good example which shows that clutch parameters are very important to reduce transmission rattle noise problem. They proposed a dry friction three-stage clutch with moderate first stage spring stiffness. Although we are using a dry clutch, the clutch examined in this study has one-stage spring set on it and this spring set is selected carefully to accommodate corresponding engine torque. It is noteworthy that three-stage clutches are not normally used with DMF systems; instead, they are used with single mass

flywheel systems due to their relatively higher rotational vibration frequencies. Furthermore, three-stage clutches are more expensive than single stage clutches due to 2 more spring sets and friction surfaces. Nonetheless, since our target should be getting the best results with a competitive price, we avoid bringing add on cost to our system.

On the other hand, analyses of longitudinal dynamic behavior of a clutch system and seeking the solution of corresponding optimization problem have not been pursued in literature. Motivated by these facts, this study is initiated in which dynamic models of components of a clutch system are derived and constructed in Matlab-Simulink, mathematical models are verified by measurements, a multi-objective optimization problem is formulated having two objective functions (i.e., pressure plate vibrations and pedal characteristics) and corresponding Pareto optimal solution is obtained and discussed. A prototype clutch is manufactured by using the design variables obtained by optimization runs and then it is tested. It is shown that analytical models agree well with the experimental measurements and vibrations in the clutch system can be reduced significantly by choosing the design parameters with optimization tools.

2. Modeling of the Clutch System

Parameters which affect axial vibrations of the clutch system will also affect clutch release load characteristics which will be discussed in the upcoming sections in detail. Since the clutch pedal load characteristics are dependent on release load characteristics, even if the vibration problem is well resolved, pedal load might be too high which may cause the clutch system becomes unusable. For that reason, clutch release load characteristics will be simulated first, and then optimization problem will be solved.

The clutch and DMF system that are the subject of this study is shown in Fig. 1. Following, dynamic models of components in this clutch system are derived. Please note that primary side of the flywheel and some internal parts could not be shown in the figure not make it more intricate.
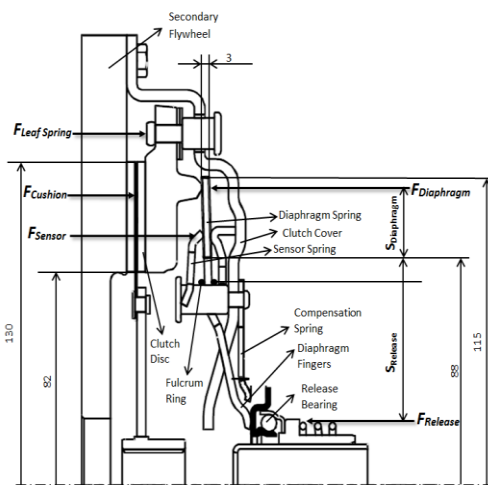

Fig. 1. Geometrical data of the simulated clutch and DMF system (at engaged position) [44].

2.1. Clutch Release Load Characteristic

Being one of the crucial elements determining the clutch dynamic behavior, clutch release load characteristic is derived from clutch release curve. A typical clutch release curve, pressure plate spring curve and lift off curve are shown in Fig. 2. While clutch diaphragm spring is the most significant component influencing clutch release load characteristic, it is also affected by leaf springs on clutch cover (which helps pressure plate disengagement), cushion springs between friction surfaces of clutch disc and clutch cover stiffness. Following sections explain how these components are modeled.

As mentioned in the abstract, two objective functions such as pressure plate vibrations and clutch pedal curve characteristic are used in this study. Clutch pedal curve characteristic is calculated by dividing the release load curve to release system's ratio and release load curve gives us the load on the release bearing as the release bearing travel changes. Note that while calculating these curves, they are modeled parametrically by using cubic spline polynomials in the mathematical model of the clutch system and employed in the optimization runs.

2.2. Diaphragm Spring

Since the diaphragm spring has two sections having completely different characteristics, it is divided into two parts and their mathematical equations are derived separately, e.g., see Fig. 3. While the disc spring is discussed below in Section 2.2.1, finger springs are studied in Section 2.4 along with the other components that are modeled by using finite element method (FEM).
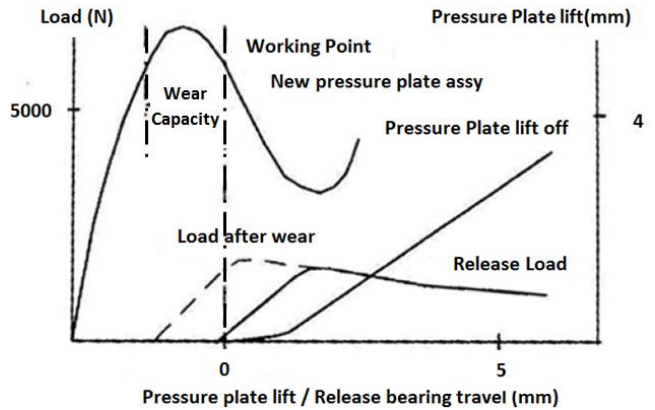

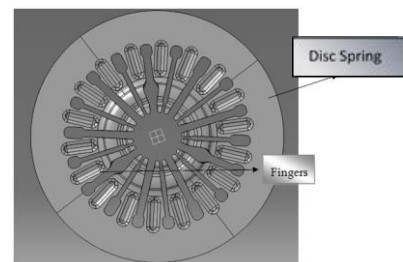**Fig. 2.** An example of a clutch pedal curve and its important points [45].

Fig. 3. Two sections of the diaphragm spring.

2.2.1. Modeling of Disc Springs.

The Almen-Laszlo formula [26] is commonly used to model the disc springs in practice [19-22].

The load P_1 acting on the outer radius of diaphragm spring can be calculated as follows:

$$P_1 = \frac{\pi E t \lambda_1 . \ln(\frac{R}{r})}{6(1-\rho^2)(L-l)^2}\left[\left(h-\lambda_1\frac{R-r}{L-l}\right)\left(h-\frac{\lambda_1(R-r)}{2(L-l)}\right)+t^2\right]$$

(2.1)

where E is the elasticity modulus of spring material, t is the thickness of diaphragm spring, λ_1 is the displacement of outer diameter of disc spring, R is the radius of outer end of disc spring, r is the inner radius of disc spring, ρ is the Poisson's ratio of spring material, L is the position of load P_1, l is the diameter of wire ring and h is the internal cone height of an unloaded diaphragm spring [20].

The load P_2 acts on the inner radius of diaphragm fingers. This leads to a large deformation λ_2 on diaphragm fingers and also λ_1 on the outer radius of disc spring as shown in Figure 4a and Figure 4b. The release load P_2 is given by [20]

$$P_2 = \frac{\pi E t \lambda_1 . \ln(\frac{R}{r})}{6(1-\rho^2)(L-l)(r-r_p)}\left[\left(h-\lambda_1\frac{R-r}{L-l}\right)\left(h-\frac{\lambda_1(R-r)}{2(L-l)}\right)+t^2\right]$$

(2.2)

Where r_p is the inner radius of diaphragm fingers where release bearing connection exists [20].

The cross section of disc spring part of diaphragm spring is presented in Figure 4.b on the right without showing the diaphragm fingers, which is used to derive load equations of disc spring. The Almen-Laszlo formulas assume that the disc spring rotates around a center which can be calculated by using the following formula [31-32]

$$D_0 = \frac{D_e - D_i}{\ln(D_e/D_i)}$$

(2.3)

Then, the load on disc spring is given by

$$F = \frac{4E}{1-\rho^2}\cdot\frac{t^4}{K_1 \cdot D_0}\cdot\frac{s}{t}\cdot\left[\left(\frac{h}{t}-\frac{s}{t}\right)\cdot\left(\frac{h}{t}-\frac{s}{2t}\right)+1\right]$$

(2.4)

$$K_1 = \frac{1}{\pi}\cdot\frac{\left(\frac{\delta-1}{\delta}\right)^2}{\frac{\delta+1}{\delta-1}-\frac{2}{\ln\delta}}$$

(2.5)

Where s is the deflection of disc spring, D_e is the outer diameter of disc spring, D_i is the inner diameter of disc spring and $\delta = D_e/D_i$ [31]. The disc spring characteristic which can be found in literature [31-32] is shown in Fig. 5 as h/t ratio changes.
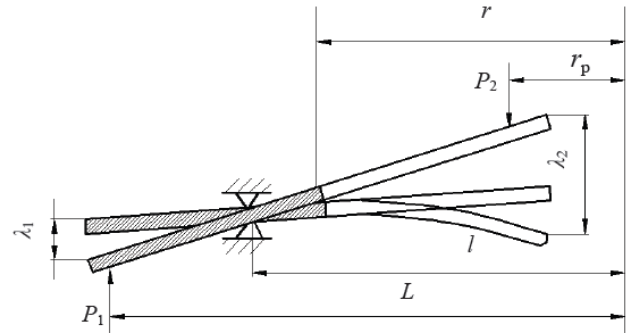

Fig.4a. Deformation of the diaphragm spring when its fingers are loaded. [20]
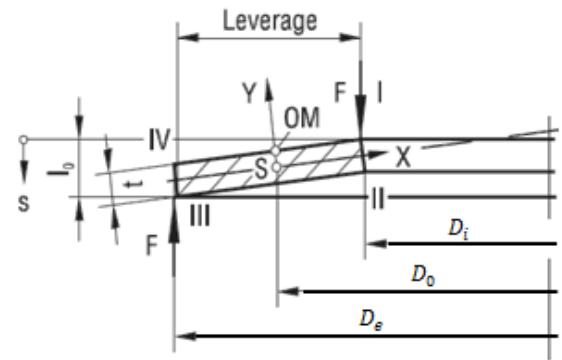

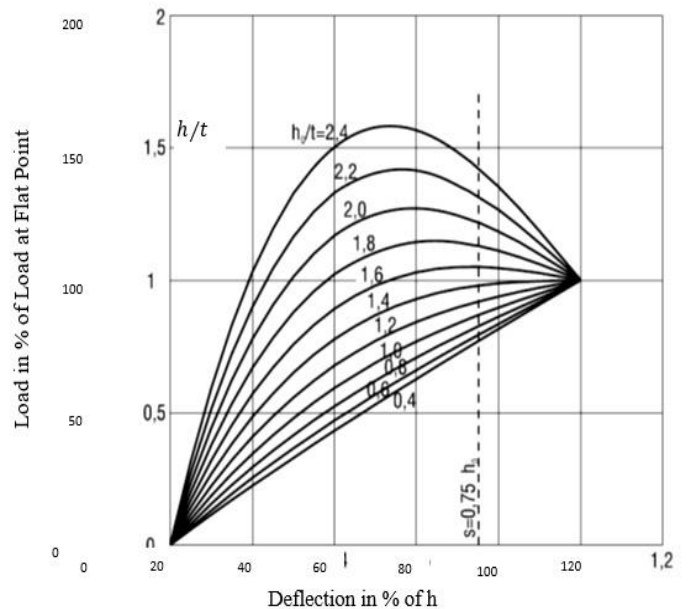**Fig..4b.** The cross section at reference position. [31]

Fig.5. Load-deflection characteristic for Belleville washers [31].

By using the formulations given above and geometrical properties of the clutch employed in this study, the clamp load curve is obtained as shown in Figure 6 where the maximum achievable load is calculated as approximately 18,000N.
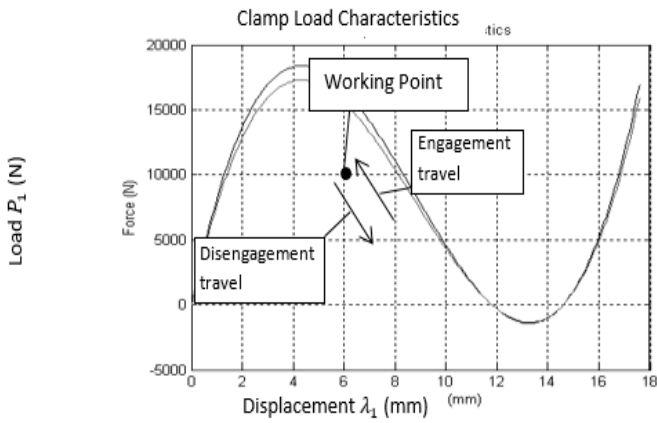
Fig.6. Clutch clamp load characteristics. The curve at the top shows the spring compression, the curve at the bottom shows the decompression phase.

Once the clamp load curve is built, operation point (λ_1) on the curve needs to be identified. In order to identify the value of λ_1, clamp load should be known which is the normal force on the clutch pressure plate at the engaged position and must be determined correctly to ensure the transmission of engine torque. A safety factor is also considered to guarantee no slippage on the clutch which is called the Slip Safety Factor (SSF) which is typically chosen as 1.2 [45]. The clamp load is calculated by using Eq. (2.7).

$$D_m = \frac{2}{3} \cdot \frac{D_e^3 - D_i^3}{D_e^2 - D_i^2} = 0.212m \qquad (2.6)$$

$$SSF\,(Slip\ Safety\ Factor) = \frac{F_{clamp} \cdot D_m \cdot \mu}{T_e} \geq 1.2 \qquad (2.7)$$

Where D_m is the diameter of gyration (centroid of friction facing surface diameter to which torque is applied to calculate the clamp load), F_{clamp} is the clamp load at the clutch operation point, μ is the friction coefficient of friction and T_e is the maximum engine torque. By the use of Eq. (2.7), the minimum clamp load is calculated as 9,400N and nominal clamp load can be selected as approximately 10,000N. Considering this clamp load, nominal operation point is calculated as 8.1mm from the Figure 6.

2.3. Modeling of Cushion Spring

The cushion spring significantly affects the release load characteristic. Its characteristic load curve used this study is shown in Figure 7 on the left [43] which is obtained from experimental measurements (e.g., see Section 3). It is parametrically modeled by using cubic spline polynomials in the mathematical model of the clutch system and employed in optimization runs. The cushion spring segment of clutch disc provides a smooth release curve and prevents large loads on the pedal load curve. In order to handle release load curve, the difference between diaphragm spring and cushion spring is calculated and divided by clutch ratio. The shaded areas in Figure 7 on the right show this difference and related release load is on the left side.
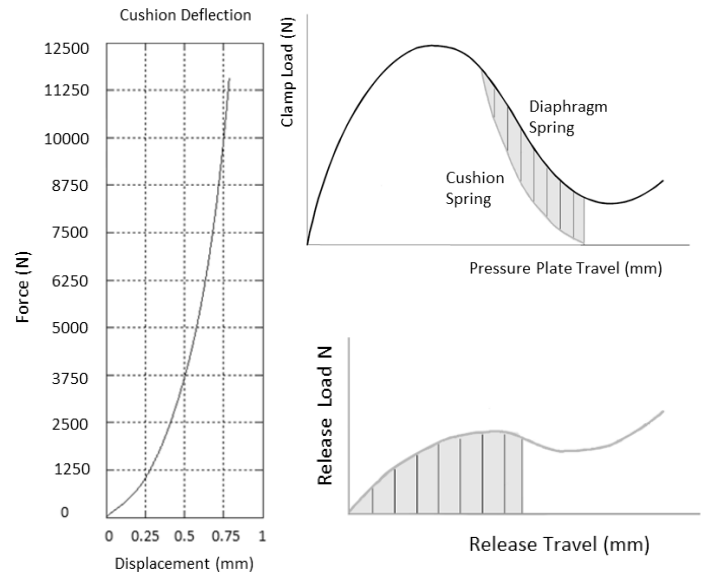

Fig.7. The cushion spring and its characteristics for the new and worn springs [43].

2.4. Modeling of Diaphragm Spring Fingers, Clutch Cover, Compensation Spring and Leaf Springs

FEM is used to model diaphragm spring fingers, clutch cover, compensation spring and leaf springs. It is noteworthy that diaphragm spring stiffness is strongly related to the clutch release load characteristic.

In order to calculate the diaphragm spring stiffness under loading, it is important to accurately model the stiffness of fingers. To this end, the slave cylinder bearing is modeled as a solid cylinder on the fingers of diaphragm springs and a contact model is defined between the bearing and fingers. There are a number of studies reported in literature used shell elements [24] or tetrahedron solid mesh elements, e.g., [49], [51-52]. Parabolic tetrahedron solid elements (with 10 nodes having three degrees of freedom (DOFs) at each node) are used in our study. In order to analyze only finger area of the diaphragm spring, all DOFs of the fulcrum ring connection are restricted as boundary conditions and distributed pressure is loaded on the release bearing. Based on FEM solutions, characteristics of fingers are found to be similar to a linear spring, which is also verified by experimental measurements, e.g., see Figure 9 (i.e., release load curve). Linear ramp up behavior of first part of the release load curve shows linear spring characteristics of diaphragm fingers. Many measurements and simulations are reported in literature on this issue, e.g., see [22], [24], [49-50].

The clutch cover stiffness is also another important parameter affecting the release load characteristic. By using parabolic tetrahedron solid elements in FEM model, distributed load is applied to fulcrum ring area and all DOFs of the bolt holes around the cover where the cover is connected to flywheel are restricted. Note that the diaphragm spring position, compensation spring position and its end stop position are different between the loaded and unloaded

30

positions of diaphragm spring. These positions change under the loading during the engagement and disengagement of clutch and significantly affect the release load curve characteristic. In order to identify these positions under different loading conditions, FEM solutions are used and relevant spring coefficients are calculated.

The compensation spring is used to achieve a more flat release load characteristic which also leads to a more flat clutch pedal characteristic. The compensation spring is activated after the maximum loading is reached during its release. After this point, the release load begins to reduce dramatically. In order to prevent this, a linear spring is used to increase the pedal loads starting from the maximum release load to the end of release bearing travel; thus, more flat pedal characteristic can be achieved [44].

Leaf springs are used to pull back the pressure plate from the clutch disc during the disengagement of clutch. These springs are thin planar plates located in front of the diaphragm spring. Due to the clamp load on the pressure plate, these plates are bent and have the function of a spring. They are only used to guarantee that the pressure plate does not touch to clutch disc after the disengagement.

In FEM models of compensation spring and leaf spring, parabolic tetrahedron solid elements with 10 nodes are used and all DOFs of rivet holes of these springs used for the connection to the cover are restricted from movement or rotation. The load between 0 to 400N is applied to leaf spring and distributed pressure is applied to the release bearing which contacts with compensation spring fingers at the release bearing travel where this contact condition is occurred.

FEM solutions of diaphragm spring, clutch cover, compensation spring and leaf spring are shown in Figure 8. Note that these results are used in the mathematical model of clutch system to derive their parametric models which is employed in the optimization runs.
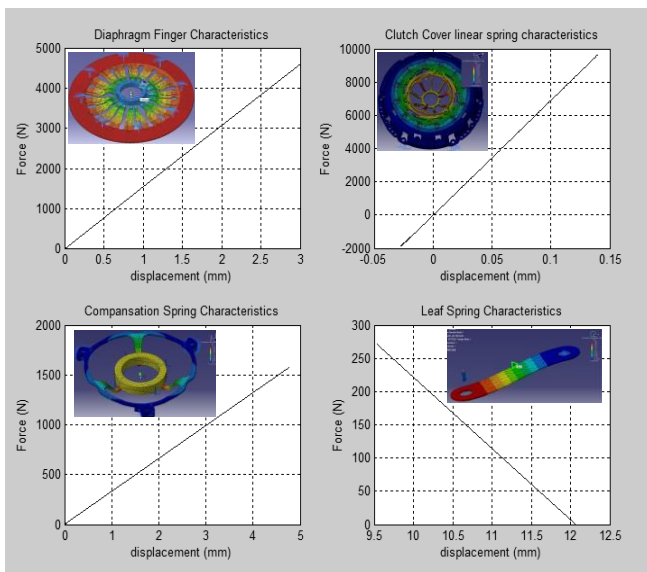

Fig.8. FEM solutions of diaphragm spring fingers, clutch cover, compensation spring and leaf springs.

The usage of FEM was necessary since the spring characteristics of subcomponents are needed separately. Experimental results give us only total system behavior as shown in c instead of handling the spring characteristics of all subcomponents separately. Furthermore, once these spring characteristics are identified, it is very easy to change the spring coefficients during optimization runs.

Once these numerical results are obtained and used in the calculations of clutch release load curve, the results are compared with experimental measurements (e.g., see Figure 9).

2.5. Derivation of Release Load Curve and Lift Off Curve

By the use of above results, we have all necessary inputs to calculate the release load characteristic and lift off curve. A simplified formulation to calculate the release load for pressure plate movement "*s*" is given by

$$F_R = \frac{F_D - F_{cushion} - F_{sensor} - F_{leaf}}{i} + F_{comp.}$$

(2.8)

where F_D is the diaphragm spring load, $F_{cushion}$ is the cushion spring load, F_{sensor} is the sensor spring load, F_{leaf} is the leaf spring load, $F_{comp.}$ is the compensation spring load which is zero at the beginning of disengagement movement of the release bearing and i is the clutch ratio. These forces are shown in Fig. 1. Then, the clutch ratio is given by

$$i = S_{Release} / S_{Diaphragm}$$

(2.9)

Where $S_{Release}$ and $S_{Diaphragm}$ are respectively distances between loads and connection rivets shown in Fig. 1.

Sensor spring load in Eq. (2.8) is created by the sensor spring shown in Fig. 1 and it increases as clutch friction faces get worn. After a certain level of load, clutch adjustment system sets in and sensor spring load decreases to the initial value. Detailed information about clutch adjustment system can be found in [44].

It can be seen in Eq. (2.8) that the clutch cover or diaphragm spring finger deflection is not considered in force equilibrium. However, while the load on these components changes during the engagement and disengagement process, their stiffness affects the positions of diaphragm fingers and subsequently the bearing position, which also determines the complete release curve characteristic. These issues are considered in the simulations to determine the mathematical model of the system and calculate the release characteristics of the clutch examined in this study.

The release load on clutch fingers and lift off curve (displacement of pressure plate and clutch finger travel) are simulated and compared with the measurements in Figure 9. These curves are the basic clutch characteristics and can be used to characterize a clutch system [45].
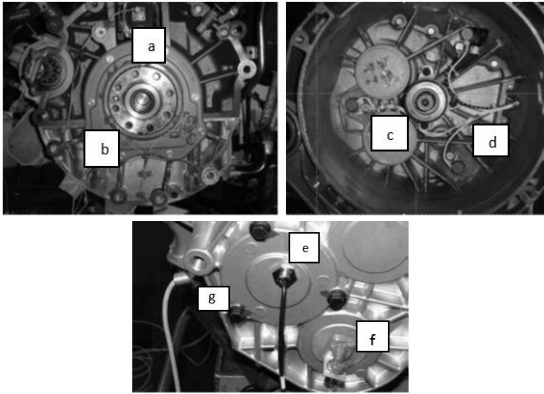
Fig.9. The release load and lift off curves.

As mentioned earlier, the release load on clutch fingers is directly related to the axial loading of clutch and load transferred to clutch pedal through clutch release system. It is observed in Figure 9 that the simulation results are very close to measurements and can be used for solving the optimization problem. Optimization results are obtained by using analytical formulas, spring characteristics of different sub-components which are obtained by FEM and parametric curve of cushion spring. Measurements are obtained by the clutch test bench which is explained in detail in Section 3.1..

3. Test Benches and Test Procedures

3.1. Load and Travel Measurement

Figure 10 shows the clutch test bench and component layouts for release load, release travel, clutch pedal load and pressure plate travel measurements. Load sensors are PULS HT1 series compression load cell type of 50kN capacity. Travel sensors are Alfa Electronic TLM type magnetostrictive displacement sensor with +/-30 μm precision.

Fig. 4. Test rig.

System components of the test bench shown in Fig. 10 are as follows

a) Clutch pressure plate, disc, bearing, fork

b) Clutch slave cylinder push rod

c) Clutch slave cylinder

d) Clutch pipe end fitting

e) Clutch hydraulic pipe

f) Master cylinder

g) Clutch pipe end fitting

h) Reservoir

i) Clutch pedal push rod

j) Clutch pin point

k) Clutch pedal

Sensors on the test bench shown in Fig. 10 are as follows

1. Force measurement from pressure plate

2. Displacement measurement from pressure plate

3. Force measurement from clutch slave cylinder push rod

4. Displacement measurement from clutch slave cylinder

5. Pressure measurement from clutch slave cylinder inlet (50 bar clutch hyd. DOT4)

6. Thermocouple on clutch pipe

7. Pressure measurement from clutch master cylinder Outlet

8. Force measurement from clutch pedal

9. Displacement measurement from clutch pedal

3.2. Dynamic Vibration Measurements

In order to measure and understand the vibration phenomena in the clutch and flywheel system, a number of displacement and speed sensors and one microphone are equipped on a transmission and engine, and these instrumented parts are used on a vehicle to measure the rattle noise and vibrations on the clutch and flywheel system. Sensor numbers and positions are listed below and shown in Fig. 11.

Measurements are performed while driving the vehicle. Firstly, the engine is accelerated above 3500 RPM, then clutch pedal is depressed (i.e., clutch disengagement). Clutch pedal is released again in one second and the clutch is allowed to engage. Rattle noise and vibration signals of components in the clutch are recorded during the clutch engagement. Note that the rattle noise is irrespective of gear position.

The noise measurement data recorded with the microphone which is at the end of the transmission housing is shown in Fig. 12 on the left where it is observed that around the engine speed of 2500 RPM is the worst possible range for the emergence of rattle noise.

Fig. 11. Locations of displacement and speed sensors for vibration analysis: a) 3 displacement sensors for crankshaft vibrations at r = 58mm , b)3 displacement sensors for primary flywheel vibrations at r = 140mm, c) 3 displacement sensors for secondary flywheel vibrations at r = 97mm d)3 displacement sensors for pressure plate vibrations at r = 118mm,e) 1 displacement sensor at the end of the transmission housing, f) 1 microphone at the end of the transmission housing (bandpass filter 1000-20000 Hz). g) 1 speed sensor for the transmission input shaft speed
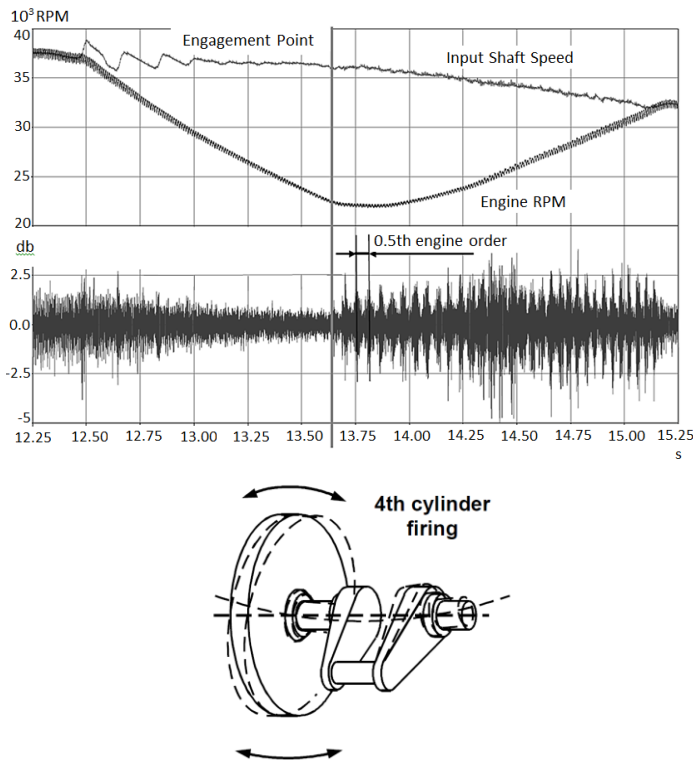
Fig. 12. Recorded noise data between 2000-3500 RPM range. Rattle noise exists at the 0.5th engine order (on the left) corresponding to crankshaft bending vibration resulting in axial clutch vibrations (on the right) [33], [46].

As mentioned in Section 1, references [33], [46], [47] reported that axial clutch vibrations are excited by the 4th cylinder of engine at the 0.5[th] engine order. Measurements tell us the rattle noise in our experimental setup occurred at the 0.5[th] engine order which is excited by the crankshaft bending vibrations which is verified by the references as shown in Figure 12 on the right side.

Figure 13 shows the measurements taken from the engine crankshaft, flywheel, clutch cover and pressure plate. It is observed in this figure that the clutch system considered in this study works like an amplifier which results in transmission rattle noise during clutch engagement.

3.3. Analysis of Vibration Modes on the Clutch and Flywheel

In order to understand the axial vibration modes of clutch and dual mass flywheel system, a modal analysis test is performed on a shaker test bench and vibrations are measured in response to axial sinusoidal excitations having 5mm release bearing travel between 0-800Hz. The shaker, instrumented clutch and test rig configuration is shown in Fig.14.

Components shown in Figure 14 are listed below:

a. Shaker

b. Flywheel primary side

c. Flywheel secondary side
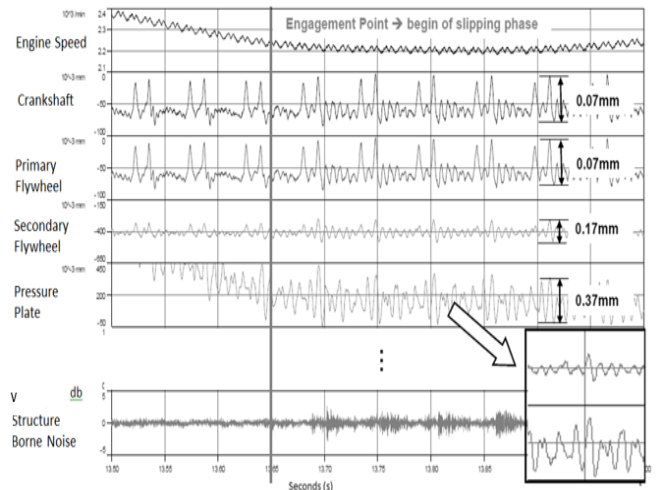
d. Pressure plate

Fig. 13. Axial vibration measurements on the crankshaft, primary and secondary flywheels and pressure plate, and its relations with rattle noise measurements.
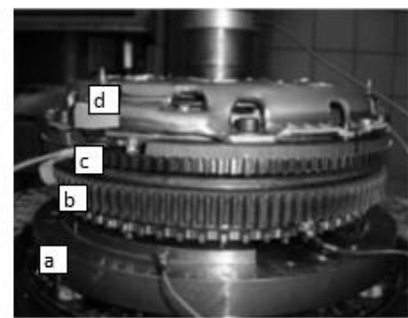

Fig. 14. Shaker test rig configuration and instrumented clutch.

Measurements obtained from this setup is presented in Fig. 20 to verify the results of mathematical results where it is observed that the first natural frequency of pressure plate is around 165Hz with a phase difference between the flywheel and pressure plate. Measurements also show that there is a second dominant frequency around 150 Hz with no phase difference between the flywheel and pressure plate whilst pressure plate shows relatively larger amplitudes in compared with the whole frequency range.

4. Mathematical Model for Pressure Plate Vibrations

Note that we have flywheel vibration measurements at hand which are excited by the crankshaft bending vibrations (especially 4th cylinder firing is effective on this kind of vibration problem (Fig. 12), e.g., see [33], [46]) and it is not possible to alter these vibrations unless the engine or cranking system is modified. Therefore, flywheel vibrations are used as an input to the vibration model of clutch system in this study.

On the other hand, in order to model the pressure plate axial vibrations, the system is modeled by the components such as the clutch disk, input shaft, pressure plate, diaphragm spring, clutch fingers and clutch cover. Engine vibration transmitted through this flywheel connection is the only source for clutch pressure plate vibration. Such a mathematical model for another clutch system can be found in [33] where a cable clutch system with an external slave cylinder and a lever system is modeled while the model in this study is a hydraulic system with a concentric slave cylinder.

The components of clutch system are shown in Fig. 1. The mathematical model includes the geometrical and physical properties of these sub-components and stiffness properties of the springs. Since excessive vibrations of the pressure plate occur during the engagement (while releasing the clutch pedal), we will simulate the system starting from the disengaged position to the engaged position; that is, this model will be working at the time while the clutch pedal is being released.

It must be underlined that this model is only built to study longitudinal vibrations of the clutch system and no rotational motion is considered. There are two main reasons for this assumption.

• If there are unexpected rotational vibrations in the engine, the noise phenomena would occur at idle or driving conditions as well. Instead, the noise is only heard during engagement phase in which pressure plate does not complete its full travel. Following, the excessive axial vibration causes pressure plate to press the clutch disc intermittently, then torque fluctuation is transmitted to the transmission that causes the rattle noise phenomena.

• Torque fluctuations can also be improved by modifying rotational dampers slightly. But this does not resolve the main source of vibration, only damps out the vibration transmitted to the transmission. This may also cause a negative effect on the dampers life time due to the vibrations on pressure plate.

Simulation results will be compared with the measurements and above mentioned assumption will be proven with the comparisons.

The simplified model of the system is shown in Fig. 15 in which diaphragm fingers are connected to the cover which can rotate around the fulcrum ring connection points. This is completely in line with the detailed representation of the clutch system shown in Fig 1; clutch disc is assumed to be consisting of two separate friction discs. The mass of these friction discs are equally added to the secondary side of flywheel and pressure plate. The cushion spring and its friction surface are shown in the model as a sub-component of the clutch disc.

In Figure 15 on the top side, experimental measurements taken from the engine is shown. As it can be seen from physical measurements, the crankshaft has two main peaks which are due to the 3rd and 4th cylinder firings which cause the crankshaft bending. These two peaks are repeated in every 720° of crankshaft rotation and used as inputs in the simulation model as shown in the same figure.

By using the simplified model shown in Figure 15, the mathematical model is obtained by using MATLAB software. To this aim, the Simulink® which is a MATLAB tool is employed that helps simulate such vibration models. The high level Simulink model for the pressure plate and clutch cover is shown in Figure 16 on the left.
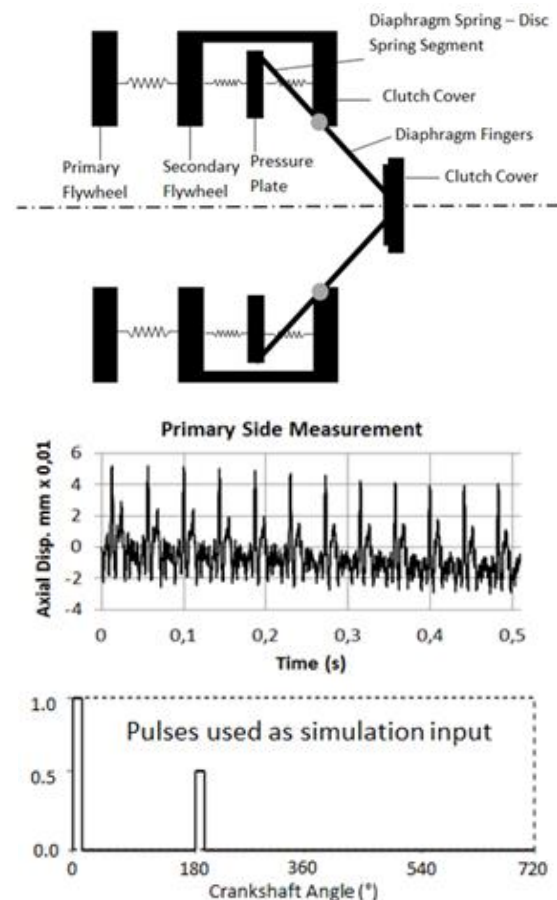

Fig. 15. Simplified model of the clutch system by considering axial vibrations and primary side axial vibrations.
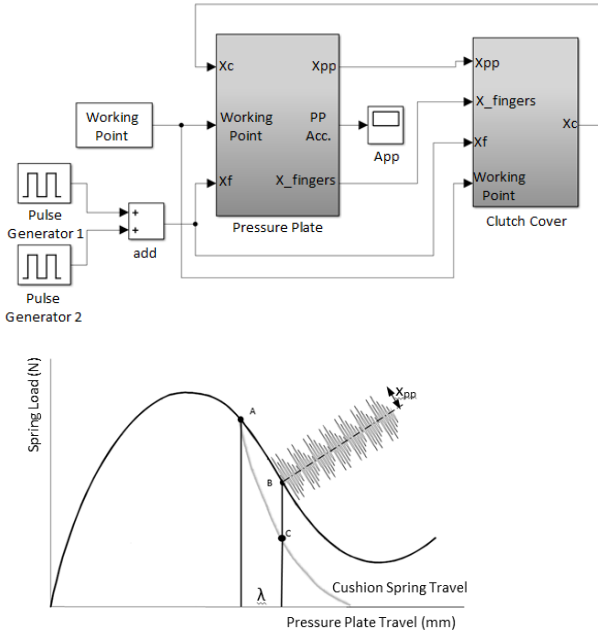
Fig.16. High level Simulink model on the left and pressure plate vibration during engagement phase on the right.

The model shown in Figure 16 has two pulse generators as explained in Figure 15, which simulate the engine excitation and is used as an input to the pressure plate and clutch cover. The main purpose is to find the pressure plate excitations. Following, simulation results will be compared with measurements.

In order to build sub-models, the mathematical equations should be obtained for vibrations. The following dynamic equations are of the system shown in Figure 15. Vibrations of the pressure plate are shown in Figure 16 on the right where point A shows the engaged position of the pressure plate (operation point), point B represents the disengagement phase at pressure plate travel λ, and point C shows the cushion spring loading at pressure plate travel λ.

$$m_{pp}\ddot{x}_{pp} + F_{disc\_spring} - F_{cushion} - F_{fingers} = 0 \quad (4.1)$$

$$m_{c}\ddot{x}_{c} - F_{cushion} + F_{R} + k_{c} \times (x_{c} - x_{f}) = 0 \quad (4.2)$$

Where m_{pp} is the pressure plate mass, $\ddot{x}_{pp}$ is pressure plate acceleration, x_{pp} is the pressure plate travel around point B in Figure 15, λ represents pressure plate travel from the point where pressure plate vibrations are calculated, F_{disc_spring} is the load on the disc spring, $F_{cushion}$ is the load on the cushion spring, $F_{fingers}$ is the load on the pressure plate created by the release load, m_{c} is the cover mass, $\ddot{x}_{c}$ is the cover acceleration, x_{c} is the cover displacement, F_{R} is the release load on the diaphragm fingers, k_{c} is the cover stiffness given in Figure 8 and x_{f} is the secondary flywheel displacement. Now, we will write the terms in Eqs. (4.1) and (4.2) with known parameters as follows

$$F_{disc\_spring} = F_{diaph}\left(\lambda + x_{pp} - x_{c}\right) \quad (4.3)$$

Where $F_{diaph(.)}$ is the clamp load at any x_{pp} (characteristic load curve for F_{diaph} is shown in Figure 6). Moreover,

$$F_{cushion} = F_{cush}\left(\lambda + x_{pp} - x_{f}\right) \quad (4.4)$$

Where $F_{cush(.)}$ is the cushion spring load at any x_{pp} which is given in Figure 7. In addition,

$$F_{fingers} = F_{R} \times i = F_{release}\left(x_{release} - x_{c}\right) \times i \quad (4.5)$$

Where $F_{release(.)}$ is the release load characteristic dependent on release travel given in Figure 9, $x_{release}$ is the release bearing travel at $(\lambda + x_{pp})$ pressure plate travel and i is the clutch ratio. We can write this equation with x_{pp} by using lift off curve which is also given in Figure 9 as follows

$$x_{release} = k_{lift}\left(\lambda + x_{pp}\right) \quad (4.6)$$

that results in

$$F_{fingers}\left(\lambda + x_{pp}\right) = F_{release}\left(k_{lift}\left(\lambda + x_{pp}\right) - x_{c}\right) \times i \quad (4.7)$$

Where $k_{lift(.)}$ is the lift off curve characteristic which gives the pressure plate travel against release travel shown in Figure 9 on the right. We can also write release load F_{R} in Eq. (4.2) as follows

$$F_{R} = F_{release}\left(x_{release} - x_{c}\right) = F_{release}\left(k_{lift}\left(\lambda + x_{pp}\right) - x_{c}\right) \quad (4.8)$$

Then, Eq. (4.1) and Eq. (4.2) become as follows

$$m_{pp}\ddot{x}_{pp} + F_{diaph}\left(\lambda + x_{pp} - x_{c}\right) - F_{cush}\left(\lambda + x_{pp} - x_{f}\right)$$
$$-F_{release}\left(k_{lift}\left(\lambda + x_{pp}\right) - x_{c}\right) \times i = 0 \quad (4.9)$$

$$m_{c}\ddot{x}_{c} - F_{cush}\left(\lambda + x_{pp} - x_{f}\right) + F_{release}\left(k_{lift}\left(\lambda + x_{pp}\right) - x_{c}\right)$$
$$+k_{c} \times (x_{c} - x_{f}) = 0 \quad (4.10)$$

After deriving the differential equations, we are ready to build the corresponding Simulink models. Since we have a number of non-linear springs and tables, it will be easier to solve the equations in time domain by using the Simulink blocks. Once these equations are solved in time domain, it is easier to examine the solutions in frequency domain.

The mathematical model has the input of 2500 RPM which is in the range such that the rattle noise is in the most noticeable range (i.e., Figure 12). The Simulink sub-models for the pressure plate and clutch cover are shown in Figure 17. These Simulink models help us solve the nonlinear differential equations given by Eq.(4.9) and Eq.(4.10). Simulation results are presented in Figure 18.

Simulink model of the pressure plate is built by using the equation of the pressure plate. The model accepts flywheel vibrations (Figure 15) and pressure plate operation point (Figure 6) as the inputs and then calculates the pressure plate vibrations x_{pp} and diaphragm finger vibrations.

Fig. 18. Comparison between simulation results (on the top) and measured vibrations (on the bottom).
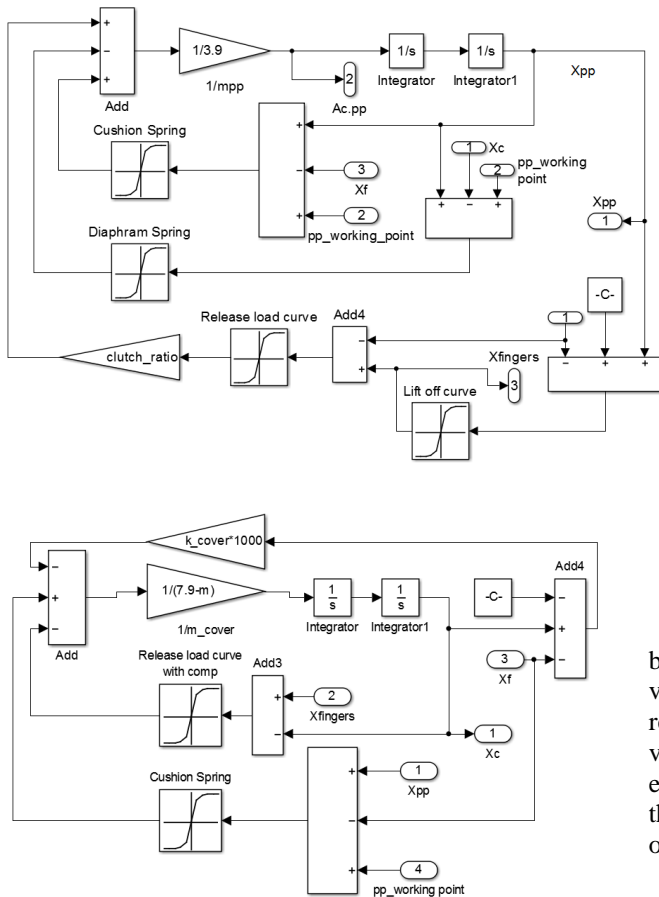
Fig. 17. Simulink models for the pressure plate (on the top) and clutch cover (on the bottom).

The model calculates every parameter in Eq. (4.9) by using cushion spring, diaphragm spring and release load characteristics which were explained in Section 2, e.g., see Figure 17 on the top.

Following Simulink model of the clutch cover is constructed by using the equation of the cover. The model accepts pressure plate and diaphragm finger vibrations from the previous Simulink model, pressure plate operation point and flywheel vibrations as the inputs and then calculates the clutch cover vibrations. The model calculates every parameter in Eq. (4.10) by using cushion spring and release load characteristics which were explained in Section 2, e.g., see Figure 17 on the right.

Simulation results and experimental measurements are presented in Figure 18 where it is observed that the simulation results show a good correlation with experimental measurements that are obtained by using the test bench explained in Section 3.2.

For instance, while the vibration amplitude in simulations is approximately 0.35 mm, it is 0.37 mm in experimental measurements at 2500 RPM. As mentioned before, measured flywheel vibrations are used as the excitation data in the simulation. All measurements are sampled during the engagement phase where the rattle noise occurs.
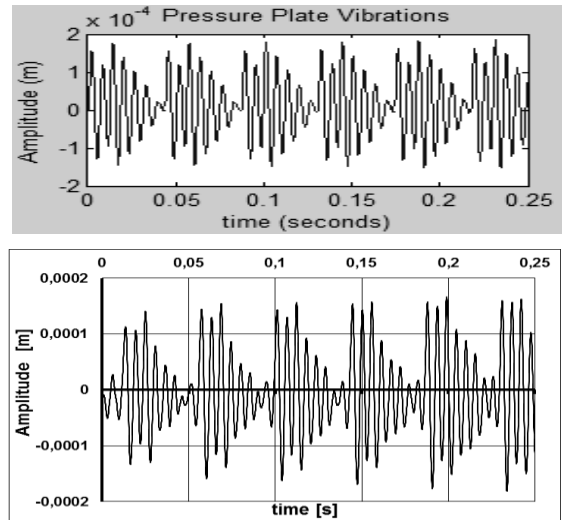
By examining Figure 18 in detail, we can observe that basically two different frequency contents exist in the vibrations. It is obvious that the signal content having relatively lower frequency is caused by the crankshaft axial vibrations which are exactly equal to the 0.5^{th} order of the engine speed. As a matter of fact, this is expected because this frequency content is one of the most critical frequencies of four cylinder engines.

If we study higher frequency vibrations in Figure 18, we observe that there is a second frequency content in the vibrations having approximately the frequency spectrum of 160Hz as shown in Figure 19 for both measured and simulated data. In sum, both measured and simulated data show a dominant frequency around 160Hz and similar sub-harmonics. The corresponding FFT analyses of measured data and simulation results show that there is another peak around 145Hz as well.
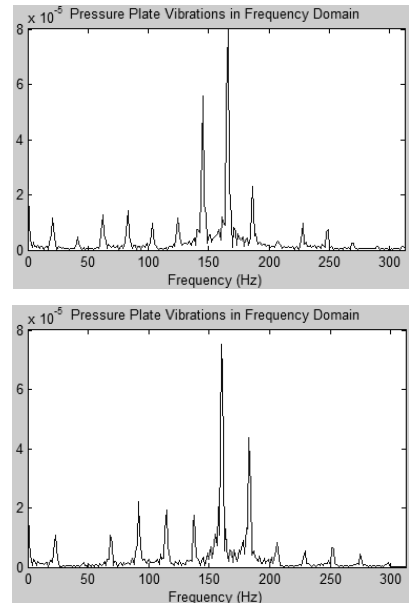

Fig. 19. Power spectrum of the pressure plate vibration measurements is on the left and that of simulation results is on the right.

Following, the shaker test is performed to find the natural frequencies of clutch system and reveal the other dominant frequencies as mentioned in Section 3.3. The frequency content of measurements during this test is given in Figure 20 in which it is observed that the first natural frequency of pressure plate is around 165Hz which also confirms our simulation results. These measurements also show that there is a second dominant frequency around 150 Hz which is also close to the observations in simulation results.

As mentioned before and shown in Figure 12, the worst range for the rattle noise problem is around 2500 RPM where the 4th engine order around this RPM is 167Hz which is very close to modal analysis and simulation results of axial pressure plate vibrations. Esfahani *et al* also reported the same results that the $0,5^{th}$ engine order excitation caused the clutch pressure plate vibration around 4th engine order frequency [33].

To sum up, these measurements are very consistent with the simulation results. R. Esfahani et al. found that the clutch pedal vibration was around 250Hz [33]. They did not investigate the reason of this vibration. The reason was most likely that natural frequency of their clutch was around this frequency value. Since the weight of the clutch they studied was 1.9kg lighter than the one we studied, it is normal that they found the natural frequency higher than what we observed.

Hasebe et al. proposed a modified clutch assembly to change the natural frequency range of the axial clutch vibrations away from the frequency range of flywheel vibrations [48]. But, they did not clearly explain which parameters were modified. In the upcoming sections, we will also identify the most critical parameters of the clutch system and optimize the vibrations of clutch set by using multi-objective genetic optimization method while keeping the clutch release loads as low as possible.
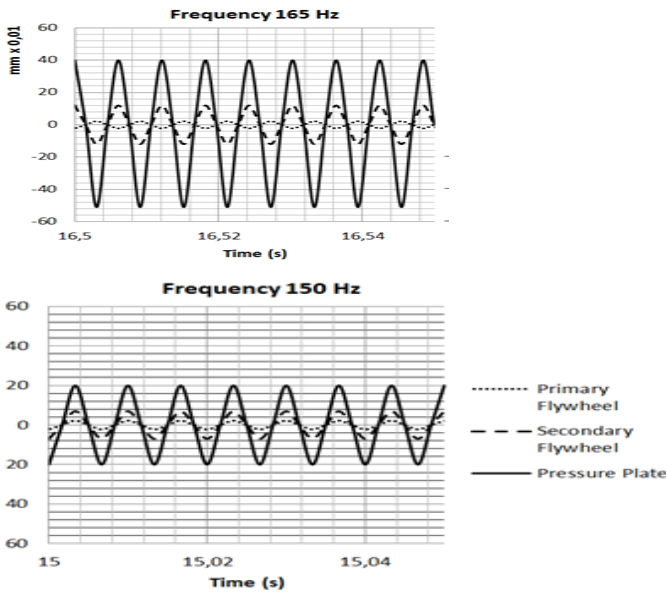

Fig. 20. Shaker test results shows that the natural frequency for clutch axial vibration is around 165 Hz and there is also a second axial dominant frequency at 150Hz.

5. Multiobjective Pareto Optimal Design of the Clutch System

In this section, a multi-objective Pareto optimal solution of the clutch system is sought by using the pedal characteristic and vibrations of pressure plate as objective functions. The first objective function is the pedal characteristic curve which is affected by a number of variables such as the geometry of diaphragm spring, material properties, release bearing stroke and dimensions of the pedal mechanism. All these variables are chosen as design variables in the related optimization problem.

The other objective function is to reduce the axial vibrations of clutch pressure plate and keep the clutch pedal load as low as possible. If design parameters are selected without considering the axial vibrations of pressure plate, excessive vibrations may emerge and cause interruptions in torque transmission during the engagement and disengagement of clutch disc. Such an interruption in torque transmission is the main cause of the well-known transmission rattle noise problem.

Note that the pressure plate mass may also be considered as an additional design variable which affects both the amplitudes of pressure plate vibrations and heat energy absorbed by clutch friction surfaces. The pressure plate mass should be as big as possible to increase the absorbed heat energy by the clutch for a longer clutch life. Thus, the heat energy absorbed by clutch friction surfaces may be considered in the Pareto optimization problem. However, it was observed in optimization runs that consideration of heat energy absorbed by clutch friction surfaces as the third objective function did not have significant effect on Pareto optimum solutions. Therefore, the heat energy absorption is calculated separately after the optimization runs are completed. Beforehand, we will investigate design variables and objective functions.

5.1. Design Variables

There are number of variables affecting the amplitudes of pressure plate vibrations and pedal characteristic. In order to understand the effectiveness of design variables on pressure plate amplitudes, sensitivity analysis is performed and the results are listed in Table 5.1 where all possible design variables and their effects on simulation results are presented.

It is noteworthy that all modifications on the clutch design will bring tooling and test costs to the relevant subcomponents. Therefore, it does not make sense to modify the variables which does not create a significant effect on the vibrations. Considering the effects of design variables on the costs, the best three options are the cushion deflection stiffness, mass of pressure plate and diaphragm spring stiffness. The diaphragm spring stiffness depends on the inner and outer diameters, thickness and its conical height.

Table 5.1. Sensitivities of variables on simulation results of pressure plate vibrations.

Variable	Increase Decrease	Effect	Magnitude of Effect
Ratio	↑↓	No significant effect	n/a
Pressure Plate Mass	↑	Improvement	Medium
Pressure Plate Mass	↓	Degradation	Medium
Leaf Spring Stiffness	↑	Improvement	Small
Leaf Spring Stiffness	↓	Degradation	Small
Clamp Load	↑	Degradation	Small
Cushion Deflection Stiffness	↓	Improvement	High
Cover Stiffness	↑	Improvement	Small
Cover Stiffness	↓	Degradation	Small
Diaphragm Spring Stiffness (h_0)	↑	Degradation	Medium
Diaphragm Spring Stiffness (h_0)	↓	Improvement	Medium

However, in comparison with other design variables, modifying only the conical height is the optimum way to modify the diaphragm spring stiffness due to the ease of tool modification and relatively lower cost. The rest of design variables would result in relatively higher costs, require major modifications on the tools (or may even need a new tool) and very big lead time.

5.2. Objective Functions and Constraints

When designing a clutch system, the first issue to be considered is to transfer the maximum engine torque to transmission system. To this end, effective clamp load should be selected carefully. Since the clamp load that is less than the required value may cause excessive slippage on the clutch system and degrades the clutch life significantly; on the other hand, the clamp load which is more than the required value may cause very high clutch pedal efforts and bad clutch feeling during the launch (e.g., very quick engagement and possible undesired stalls).

Subsequently, the first objective function should be the minimization of maximum pressure plate vibration amplitude which is the main source for rattle noise. Since the maximum vibration amplitudes are observed between the frequency range of 100 to 200 Hz (e.g., see Fig. 19 and 20), we will focus on this frequency interval for the first objective function. This frequency range also covers the 4th engine orders of the engine speed between 1500-3000 RPM range which is the critical engine order as discussed in Section 4. Moreover, as another constraint in optimization runs, the clamp load is chosen as 10,000N at the beginning of the design process which is given in the section on modeling of disc spring (i.e., Section 2.2.1).

The other basic function of the clutch system is to cut the torque transfer from the engine to transmission system when requested (to prevent stall or change transmission gear). While fulfilling this function, the maximum clutch pedal effort should be as low as possible. High pedal efforts would cause unsatisfactory drivers. Thus, the second objective function can be defined as the minimization of maximum clutch pedal effort which is directly connected with maximum release load. Considering these objective functions and constraints, the multi-objective optimization problem can be built as shown in Eq. (4.1). That is,

$$\text{minimize } x_{pp}, \text{ minimize } F_R \text{ subject to } \begin{cases} F_{clamp} >= 10000 \\ 100 < frequency < 200 \end{cases}$$

$$m_{pp}\ddot{x}_{pp} + F_{diaph}\left(\lambda + x_{pp} - x_c\right) - F_{cush}\left(\lambda + x_{pp} - x_f\right) - F_{release}\left(k_{lift}\left(\lambda + x_{pp}\right) - x_c\right) \times i$$
$$= 0$$

$$m_c\ddot{x}_c - F_{cush}\left(\lambda + x_{pp} - x_f\right) + F_{release}\left(k_{lift}\left(\lambda + x_{pp}\right) - x_c\right) + k_c \times \left(x_c - x_f\right) = 0$$

$$F_R = \frac{F_D - F_{cushion} - F_{sensor} - F_{leaf}}{i} + F_{comp.} \tag{5.1}$$

One of the functions of clutch system is to transfer the heat energy generated by the friction on disc surfaces. To this end, the clutch heat energy generation calculations are completed after the optimization runs are completed by using the following [45]

$$Q = \frac{\mu F_{clamp} V_x t_x}{2} \tag{5.2}$$

Where Q is the dissipated heat energy, μ is the friction coefficient of clutch faces, F_{clamp} is the clamp force on the pressure plate, V_x is the vehicle speed and t_x is the time.

The ratio of Q/A for the cross sectional area A is widely used to "normalize" heat generation as a sizing parameter. This normalized value is used to evaluate clutch heat effects. In addition, Q/m_{pp} for the unit pressure plate mass m_{pp} is also used when considering "heat sink" capability of clutch pressure plate [45].

Since the clutch inner or outer diameters are not chosen as optimization parameters, Q/A will not be changed. However, we need to check Q/m_{pp} since pressure plate mass m_{pp} is an optimization variable and may be changed after the optimization runs. If the pressure plate mass m_{pp} is reduced, heat sink capability of the pressure plate will be reduced (more heat energy will need to be sank into unit mass).

5.3. Optimization of The Clutch System As a Dynamic System

Since we have more than one objective function, multi-objective genetic optimization algorithm in Matlab is used in the optimization runs. The genetic algorithm is a method for solving both constrained and unconstrained optimization problems based on natural selection that drives biological evolution. The genetic algorithm repeatedly modifies a population of individual solutions. At each step, it selects individuals randomly from the current population to be parents and uses them to produce the children for the next generation. At each iteration, the genetic algorithm performs a series of computations on the current population to produce a new population. Each successive population is called a new generation. An individual is any point to which you can apply the fitness functions whose value for an individual is its score. A population is an array of individuals that consist of optimization parameters. The fitness function is the name of the optimization functions for genetic algorithm [53]. Typically, the algorithm is more likely to select parents that have better fitness values.

The genetic algorithm begins by creating a random initial population by using optimization variables. The algorithm then creates a sequence of new populations. To create the new population, the algorithm performs the following steps:

1. Scores each member of the current population by computing its fitness value.

2. Scales the raw fitness scores to convert them into a more usable range of values.

3. Selects members, called parents, based on their fitness.

4. Some of the individuals in the current population that have lower fitness are chosen as elite. These elite individuals are passed to the next population.

5. Produces children from the parents. Children are produced either by making random changes to a single parent (mutation) or by combining the vector entries of a pair of parents (crossover).

6. Replaces the current population with the children to form the next generation.

As an outcome of the above described optimization problem, a Pareto chart is created. The curve in this chart is built with optimum points for both objective functions. It means that we do not have only one optimum solution, instead we have a list of optimum solutions and we need to select one of these solutions which can serve to our aim as the best result.

It must be noted at this point that all relevant optimization parameters are modified at each optimization iterations if the geometry of clutch, mass or stiffness are varied during optimization process. Thus, each iteration is actually an independent simulation which uses new design parameters and re-calculated curves.

Figure 21 shows the Pareto chart of the clutch system and optimum solutions of clutch system. The four solutions having relatively lower values for the objective functions 1

and 2 are encircled in Figure 21, which can be selected as the optimum solution by the designer. Note that the total solution time is 840 seconds on a computer having AMD Athlon 2.8 GHz dual core processor.

As it can be seen in the Pareto chart, global optimum points are calculated as;

-   Cushion deflection under max clamp load = 0.75+0.188=0.938mm

-   Pressure plate mass = 4.0387 kg

-   Diaphragm spring conical height = 8.971mm

However, these values cannot be handled due to the tolerances of clutch manufacturing process. Reasonable values which can be manufactured by manufacturing processes can be found by rounding above design parameters as follows

-   Cushion deflection under max clamp load = 0.75+0.2=0.95mm

-   Diaphragm spring conical height = 9mm

Table 5.2 shows the comparison between the original parameters of the first physical clutch, optimized parameters and results of the objective functions.

The simulation results which are shown in Figure 22 are calculated by using the variables given in Table 5.2. If the results are compared with the initial system (e.g., Figure 18 and Figure 19), it can be observed that the vibration amplitudes of pressure plate are reduced by 0.06mm that is significant. This makes 0,12mm improvement in total pressure plate displacement which makes approximately 35% improvement on vibration amplitudes. The FFT results also show the same improvement especially around the frequency range of 140-160Hz.

Following, the physical model is produced by using the optimum design variables given in Table 5.2 and then tested. Experimental measurements obtained from the optimized clutch system are shown in Figure 23 in which it is observed that the experimental results give close results to simulation results. Both simulated and measured data have the same dominant frequency around 160Hz and their FFT results are very close to each other. The maximum amplitudes are also very close to each other (around 0,125mm-0,130mm).

Moreover, it is observed in the experiments that the rattle noise is reduced approximately 40% based on microphone measurements that can be observed if Figure 24 is compared with Figure 12. The measurements are performed as explained in Section 3.2. In brief, the simulation results and experimental measurements are encouraging and axial vibrations in the drive line are reduced by optimization process.

Finally, if we check the heat sink capability of optimized mass and compare with that of the initial mass (i.e., 3.9kg), we can see that the heat sink capability is

improved by 3.56% since the mass is increased; that is,

$$\left\{ \frac{Q}{3,9} \middle/ \frac{Q}{4,0387} \right\} \rightarrow 3,56\%$$

.

Table 5.2. Comparison of initial and optimized clutch parameters and their objective functions.

Clutch Type	Cushion Disp. (mm)	Pressure Plate mass (kg)	Diaphragm Spring Height (mm)	Max. Release load (N)	Pressure Plate Amplitudes (mm)
Initial Clutch	0,75	3,9	9,2	2250	0,185
Optimized Clutch	0,95	4,04	9	2170	0,127
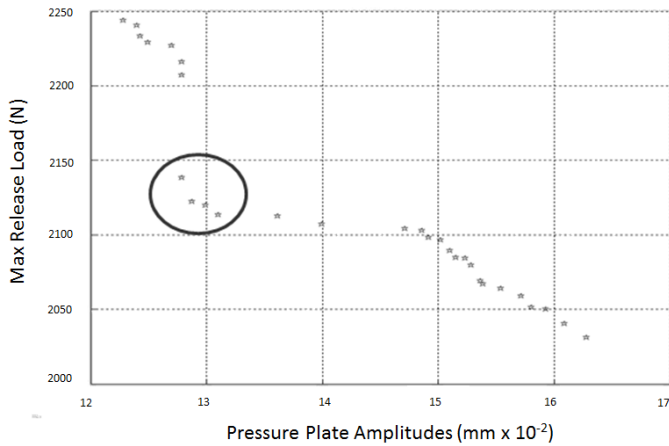
Fig. 21. Pareto chart of the optimization problem, where the objective #1 shows the pressure plate amplitude and the objective #2 shows the maximum pedal load.
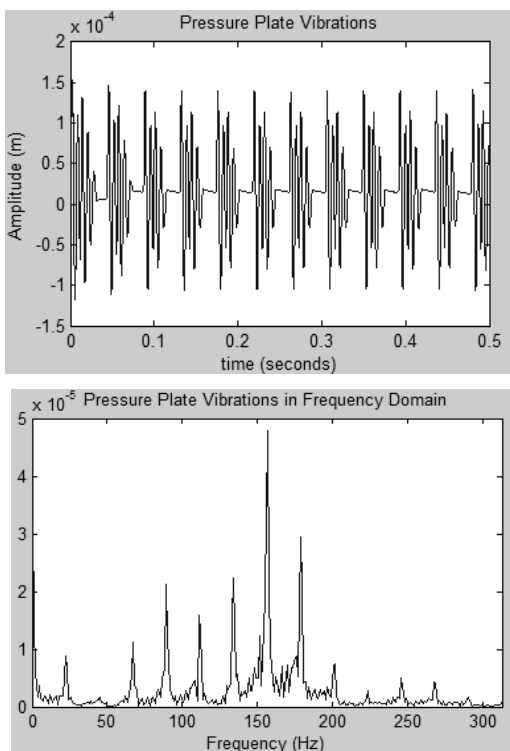
Fig. 22. Simulation results of pressure plate vibrations for the optimized clutch (in time domain on the top and in frequency domain on the bottom).
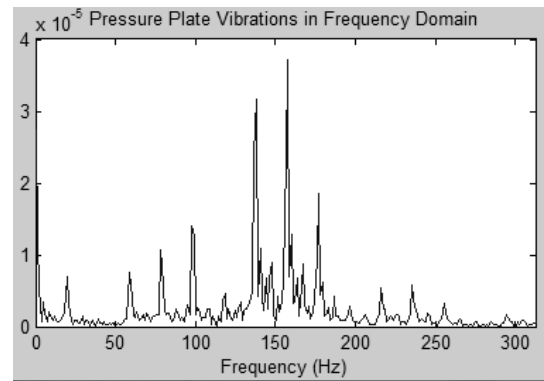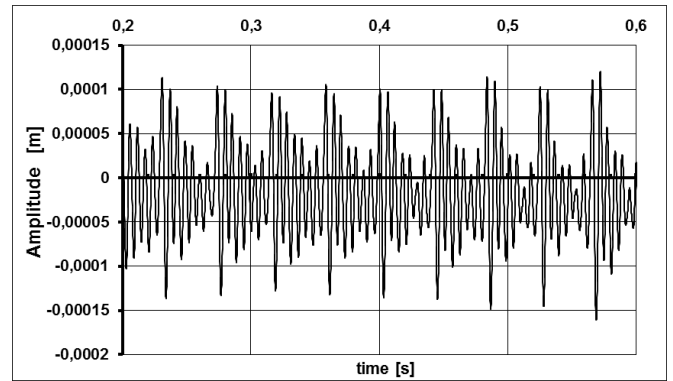

Fig. 23. Experimental measurements for pressure plate vibrations measured on the physical model produced by using optimized parameters (in time domain on the top and in frequency domain on the bottom).
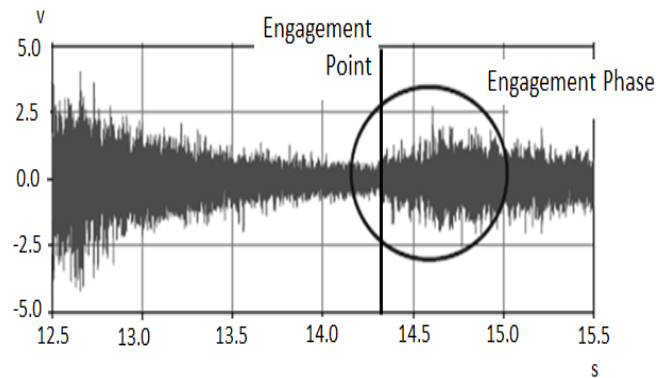

Fig. 24. Noise measurements of optimized system.

6. Conclusion

Axial vibrations in clutch systems are generally ignored in studies on dynamic behavior of clutch systems in literature, since the clutches are used to damp torsional vibrations instead of the axial ones. However, axial vibrations has to be examined for the driveline noise calculations, in particular in the existence of transmission rattle noise.

On the other hand, axial vibrations and pedal efforts are actually highly related to each other, since they are both derived by the same variables such as stiffness values of springs in the clutch and clutch ratio. To this end, mathematical models for the clutch pedal effort and clutch

pressure plate vibrations are derived and built by using the

Then, these models are verified by making comparisons with experimental measurements. By combining the simulation models together, a multi-objective optimization problem is formulated and solved such that axial vibrations and clutch pedal effort are minimized under some constraints. At the end of the study, a physical model is also produced by using the optimization results and physically tested.

It is observed that experimental measurements and simulation results are quite close to each other and axial vibrations in the drive line is reduced by optimization process. Under the light of findings of this study, it is possible to calculate and design the components of a clutch system in an optimum way, which will help decrease the test and prototype costs significantly.

On the other hand, optimizing a clutch system considering axial vibrations only will not degrade the rotational vibrations and, in order to reduce the different level of rotational vibrations from engine to transmissions (e.g., idle vibrations, creep vibrations or drive vibrations, etc…), different types of rotational dampers are used on clutch discs. However, in our study we tried to reduce the axial vibrations of disengaged clutch, thus effects of these axial vibrations during half engaged clutch position (which can be called slipping phase or engagement phase).

These axial vibrations have no influence on the system when the clutch is fully engaged since very high clamp load is already exerted on the pressure plate that prevents the axial vibrations. However, a further study may also be planned to optimize the rotational dampers so that they can be usable during engagement phase. Thus, the clutch can be optimized to minimize the axial vibrations and rotational dampers can damp the residual vibrations which cannot be fully damped by axial vibration optimization during engagement phase.

Acknowledgements

References

[1]   E. Galvagno, M. Velardocchia, A. Vigliani, Dynamic and kinematic model of a dual clutch transmission, Mech. and Mach. Theory 46 (6) (2011) 794-805.

[2]   Manish Kulkarni, Taehyun Shim, Yi Zhang, Shift dynamics and control of dual-clutch transmissions, Mech. and Mach. Theory 42 (2) (2007) 168-182.

[3]   Nowshir Fatima, Par Marklund, Roland Larsson, Influence of clutch output shaft inertia and stiffness on the performance of the wet clutch, Tribol. Trans. 56 (2) (2013) 310-319.

[4]   Y. Zhang, X. Chen, X. Zhang, H. Jiang, W. Tobler, Dynamic modeling and simulation of a dual-clutch automated lay-shaft transmission, J. of Mech. Des. 127 (2) (2005) 302-307.

programs MATLAB and MATLAB-Simulink toolbox.

[5]   Q. Zheng, K. Srinivasan, G. Rizzoni, Dynamic modeling and characterization of transmission response for rontroller resign, SAE Int. 981094 (1998) doi:10.4271/981094.

[6]   C. Pan, J. Moskwa, Dynamic modeling and simulation of the Ford AOD automobile transmission, SAE Int. 950899 (1995) doi:10.4271/950899.

[7]   Z. S. Filipi, D. N. Assanis, A nonlinear, transient, single-cylinder diesel engine simulation for predictions of instantaneous engine speed and torque, J. of Eng. for Gas Turbines and Power. 123 (4) (2001) 951-959.

[8]   E.M. Mockensturm, E.M. Balaji, Piece-wise linear dynamic systems with one-way clutches, J. of Vib. and Acoust 127 (5) (2005) 475-482.

[9]   F.R. Zhu, R.G. Parker, Non-linear dynamics of a one-way clutch in belt-pulley systems, J. of Sound And Vib. 279 (1-2) (2005) 285-308.

[10]   T. Petrun, J. Flasker, M.A. Kegl, *Friction model for dynamic analyses of multi-body systems with a fully functional friction clutch*, J. of Multibody Dyn. 227 (2) (2012) 89-105.

[11]   A. R. Crowther, N. Zhang, Torsional finite elements and nonlinear numerical modelling in vehicle powertrain dynamics, J. of Sound and Vib. 284 (3) (2005) 825-849.

[12]   C. Duan, R. Singh, Influence of harmonically varying normal load on steady-state behavior of a 2dof torsional system with dry friction, J. of Sound and Vib. 294 (3) (2006) 503-528.

[13]   C. Duan, R. Singh, Dynamics of a 3dof torsional system with a dry friction controlled path, J. of Sound and Vib. 289 (4) (2006) 657-688.

[14]   C. Padmanabhan, R. Singh, Influence of clutch design on the reduction and perception of automotive transmission rattle noise, Noise-Con 93 (1993) 607-612.

[15]   H. Moradi, H. Salarieh, Analysis of nonlinear oscillations in spur gear pairs with approximated modelling of backlash nonlinearity, Mech. and Mach. Theory 51 (2012) 14-31.

[16]   T. C. Kim, T. E. Rook, R. Singh, Super - and sub-harmonic response calculations for a torsional system with clearance nonlinearity using the harmonic balance method, J. of Sound and Vib. 281 (3) (2005) 965-993.

[17]   T. C. Kim, T. E. Rook, R. Singh, Effect of nonlinear impact damping on the frequency response of a torsional system with clearance, J. of Sound and Vib. 281 (3) (2005) 995-1021.

[18]   J. Awrejcewicz, D. Grzelczyk, Modeling and analytical/numerical analysis of wear processes in a mechanical friction clutch, Inter. J. of Bifurc. and Chaos 21 (10) (2011) 2861-2869.

[19] W. Zhang, G. Zhu, Research and application of PSO algorithm for the diaphragm spring optimization, Forth Inter. Conf. on Nat. Comput. (2008) 549-553.

[20] W. Yong-hai, Multi-objective optimization design of vehicle clutch diaphragm spring, Second Inter. Conf. on Intell. Comput. Technol. and Autom. (2009) 194-197.

[21] X. Guo, H. Lu, Optimal design on diaphragm spring of automobile clutch, Second Inter. Conf. on Intell. Comput. Technol. and Autom. (2009) 206-208.

[22] A. Li-jun, L. Tao, S. Bao-yu, Optimum design of automobile diaphragm spring clutch, IEEE Veh. Power and Propuls. Conf. (2008) 1-4.

[23] G. Ercole, G. Mattiazzo, S. Mauro, M. Velardocchia, F. Amisano, G. Serra, Experimental methodologies to determine diaphragm spring clutch characteristics, SAE Int. (2000) 10.4271/2000-01-1151.

[24] W. Nam, C. Lee, Y. Chai, J. Kwon, Finite element analysis and optimal design of automobile clutch diaphragm spring, SAE Int. (2000) 2000-05-0125.

[25] W. Jin, Solid modeling and finite element analysis of diaphragm spring clutch, Manag., Manuf. and Mater. Eng 452-453 (2012) 258-263.

[26] J. O. Almen, A. Laszlo, The uniform section disk spring, *ASME 58 (*1936) 305-314.

[27] G. Wempner, Axisymmetric deflections of shallow conical shells, J. of Eng. Mech. 90 (2) (1964) 181–194.

[28] G. Curti, M. A. Orlando, New Calculation of Coned Annular Disk Spring, ASME Winter Annual Meet. (1976).

[29] Y. Zhiming, Y. Kaiyuan. A Study of Belleville Spring and Diaphragm Spring in Engineering. J. of Appl. Mech. 57 (4) (1990) 1026-1031.

[30] S. Ozaki, K. Tsuda, J. Tominaga, Analyses of static and dynamic behavior of coned disk springs: effects of friction boundaries, Thin-Walled Struct. 59 (2012) 132-143

[31] E. Fromm, W. Kleiner, Handbook for Disc Springs, Heilbronn, SCHNORR, 2003.

[32] J. E. Shigley, C. Mischke, Standart Handbook of Machine Design, third ed., McGraw-Hill, San Francisco, 2004.

[33] R. Esfahani, A. Farshidianfar, A. Shahrjerdi, F. Mustapha, Longitudinal vibrations analysis of vehicular clutch, Aust. J. of Basic and Appl. Sci. 3 (4) (2009) 3633-3641.

[34] R. Singh, H. Xie, R. J. Comparin, Analysis of automotive neutral gear rattle, J. of Sound and Vib. 131 (2) 1989 177-196.

[35] S. Theodossiade, O. Tangasawi, H. Rahnejat, Gear teeth impacts in hydrodynamic conjunctions promoting idle gear rattle, J. of Sound and Vib. 303 (3) (2007) 632-658.

[36] E. Rocca, R. Russo, Theoretical and experimental investigation into the influence of the periodic backlash fluctuations on the gear rattle, J. of Sound and Vib. 330 (20) (2011) 4738-4752.

[37] Y. Kadmiri, E. Rigaud, J. P. Laudet, L. Vary,

Experimental and numerical analysis of automotive gearbox rattle noise, J. of Sound and Vib. 331 (13) (2012) 3144-3157.

[38] M. Barthod, B. Hayne, J. L. Tebec, J. C. Pin, Experimental study of gear rattle excited by a multi-harmonic excitation, Appl. Acoust. 68 (9) (2007) 1003-1025.

[39] X. Wang, B. L. B. Gadegbeku, L. Bouzon, Biomechanical evaluation of the comfort of automobile clutch pedal operation, Int. J. of Ind. Ergon. 34 (3) (2004) 209-221.

[40] A. Shabibi, Solution of heat conduction problem in automotive clutch and brake systems, Proc. of 2008 ASME Summer Heat Transf. Conf. 321 (2008).

[41] A. R. Crowther, C. Janello, R. Singh, Quantification of clearance-induced impulsive sources in a torsional system, J. of Sound and Vib. 307 (3-5) (2007) 428-451.

[42] C. Duan, R. Singh, *S*uper-harmonics in a torsional system with dry friction path subject to harmonic excitation under a mean torque, J. of Sound and Vib. 285 (4-5) (2005) 803-834.

[43] W. Reik, The self-adjusting clutch – SAC, 05th LuK Symp. (1994) 43-62.

[44] K. L. Kimming The Self-Adjusting Clutch SAC of the 2nd Generation, LuK Symp. (1998) 5-22.

[45] R. Shaver, Manual Transmission Clutch System, first ed., Warrendale: SAE, (1997), p: 28, 59-63.

[46] A. Reitz, J. W. Biermann, P. Kelly, Special Test Bench to Investigate NVH Phenomena of the Clutch System, Inst. für Kraftfahrwesen Aachen

[47] P. Kelly, H. Rahnejat, Clutch Pedal Dynamic Noise and Vibration Investigation, Proc. of the 1st Int. Symp. on Multi-Body Dyn.: Monit. and Simul. Tech., Bradford, UK, MEP Press, 1997

[48] T. Hasabe, U. A. Seiki, Experimental Study of Reduction Methods for Clutch Pedal Vibration and Drive Train Rattling Noise from Clutch System, SAE Int. 932007 (1993). doi:10.4271/932007

[49] M. Özbakış, Observation and optimization of the characteristic of the diaphragm springs used in clutch systems, Master Thesis, Dokuz Eylül University, Turkey, 2008.

[50] A. Hagerodt, F. Küçükay, Optimum Design of Return and Cushion Springs for Automatic Transmission Clutches, SAE Int. 2001-01-870 (2001)

[51] V. Arora, G. Bhushan, M. L. Aggarwal, Eye Design Analysis of Single Leaf Spring in Automotive Vehicles Using CAE Tools, Int. J. of App. Eng. And Tech. 1 (1) (2011) 88-97.

[52] V. Arora, M. L. Aggarwal, G. Bhushan, A Comparative Study of CAE and Experimental Results of

Leaf Springs in Automotive Vehicles, Int. J. of Eng. Sci. and Tech. 3 (9) (2011) 6856-6866.

[53]   Genetic Algorithm and Direct Search Toolbox™ User's Guide, Natick, The MathWorks, Inc, (2009), p:48.